MP140317
MITRE PRODUCT

MITRE

Modeling and Analysis of Gated, Pulsed RFI and Its Effect on GPS Receivers

Analysis of Average Cycle Slip Rate and Average Bit Error Probability

Keith R. Santarelli
David S. Choi
April 2014

Sponsor: SMC/GPE
Dept. No.: J82C
Contract No.: FA8702-14-C-0001
Project No.: 03146SC0-SE

Bedford, MA

This page intentionally left blank.

Abstract

We develop two new models for gated, pulsed radio frequency interference (RFI), one for cycle slip performance, and one for bit error performance. We compare the results of these two models to an existing, approximate model that is currently present in ITU-R Report M.2220, herein referred to as the dynamic duty cycle factor (DDCF) model. After deriving our new models, we show through case studies that the new time-varying models often predict much worse performance than the corresponding DDCF counterparts. We therefore conclude that further investigation (either by simulation or laboratory measurement) is warranted to verify the new models presented herein.

Keywords: pulsed RFI, cycle slips, bit errors, duty cycle.

This page intentionally left blank.

Table of Contents

List of Figures

List of Tables

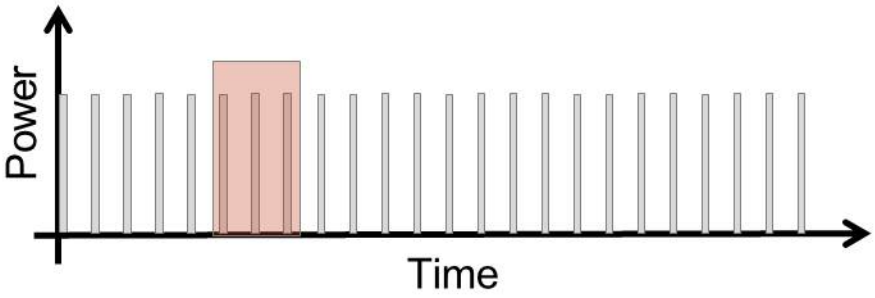

Figure 1: Graphical depiction of pulsed RFI model. The red box depicts a window of time over which C/N_0 is averaged to produce an estimate of the degraded C/N_0.

1 Introduction

Pulsed Radio Frequency Interference (pulsed RFI) is a phenomenon that can degrade the performance of GPS receivers [1]—[9]. When strong pulses that lie within the GPS band are present at the input of a GPS receiver, the input often saturates, which has the effect of masking any useful data during the time periods that the pulses are present. The effect of the pulses on system performance is a function of the receiver type (e.g., blanking vs. non-blanking, fast vs. slow), and, hence, a significant amount of effort has been put into modeling the effect of pulsed RFI on various receiver types.

Recommendation ITU-R M.2030 [1] provides a set of models for calculating the degradation effects of pulsed RFI by computing an equivalent continuous wave (CW) noise interference that lowers the nominal carrier-to-noise density C/N_0. A nominal depiction of pulsed RFI interference that is considered in M.2030 is shown in Fig. 1. Here, the pulses are assumed to occur with a regular pulse repetition frequency (PRF). The post-correlator effective degradation on C/N_0 for a saturating receiver as a function of the pulse duty cycle PDC is [1]:

$$\Delta C/N_0 = 20\log(1 - PDC) \quad (1)$$

$$PDC \triangleq PW \times PRF \quad (2)$$

where PW represents the pulse width (sec) and PRF is the pulse repetition frequency. Eqn. 1 represents a theoretical model of how to estimate C/N_0 degradation, while the red box in Fig. 1 shows how one might compute this degradation via measurement. Instantaneous C/N_0 values would be obtained inside the window and the results would be averaged to obtain a crude estimate of C/N_0 when the pulsed RFI is present. If the pulsed RFI is persistent, it is easy to see from the figure that the average value of C/N_0 is roughly independent of the placement of the window and, therefore, the estimate of C/N_0 is an approximately time-invariant quantity. Therefore, it seems reasonable to use this model of degraded C/N_0 as an indicator for the four basic GPS receiver functions (namely acquisition, carrier tracking, code tracking, and data demodulation).

NASA has proposed a plan to introduce a spaceborne scatterometer for its Solid Moisture Active Passive (SMAP) Program that will be operating in the L2 frequency band [10]. GPS receivers operating in this band are subject to corruption, and NASA is obliged to show that their scatterometer

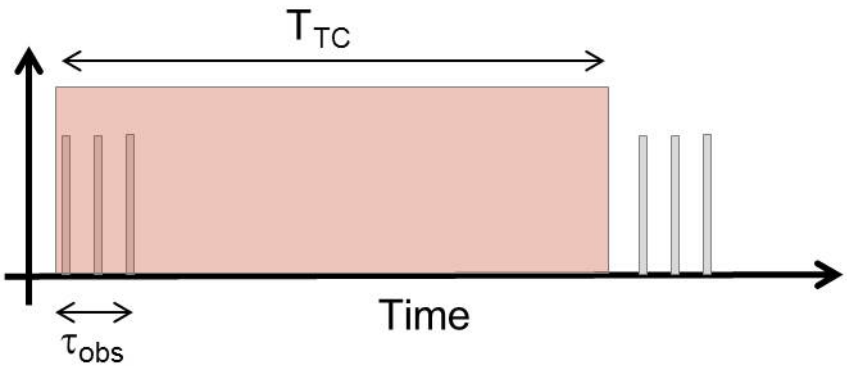

Figure 2: Pulsed RFI waveform with gating. The pulses are present for τ_{obs} seconds and are absent for the remaining $T_{TC} - \tau_{obs}$ seconds.

will not significantly degrade the performance of a GNSS receiver as compared to ambient operation. The scatterometer system uses a mechanical rotating antenna, which can illuminate a victim GPS receiver for a short time (τ_{obs} = 300 msec) during each rotation period (T_{TC} = 4.1 sec). A graphical depiction of this new type of pulsed RFI waveform, where the pulsing is *gated* to model the fact that the high frequency pulses will only be present at the receiver for 300 msec, is shown in Fig. 2. There is a single sentence in ITU-R Report M.2220 which states that the corresponding degradation in C/N_0 should now be modeled as

$$\Delta C/N_0 = 20\log(1 - PDC_{LIM}) \quad (3)$$

$$PDC_{LIM} \triangleq PDC\frac{\tau_{obs}}{T_{TC}}. \quad (4)$$

The degradation model of Eqn. 3 and 4, herein referred to as the *Dynamic Duty Cycle Factor (DDCF) model*, states that one can view the gated pulsed RFI waveform as having a composite duty cycle that is the product of the duty cycle of the pulsed waveform (PDC) and the duty cycle of the of the gating waveform (τ_{obs}/T_{TC}). While such a model is clearly convenient, its applicability to modeling the real-world effects of such a pulsing waveform is questionable. Effectively, Eqn. 3 states that the effective degradation in C/N_0 can be computed by averaging the C/N_0 values in the long red window of Fig. 2. While the instantaneous degradation may be large during the τ_{obs} seconds that the pulsing is present, the remaining $T_{TC} - \tau_{obs}$ seconds of quiescent behavior have the potential to hide the negative contributions of the pulsing waveform when the long term average is taken. It is possible —and in fact, quite likely—that the negative effect of the pulses during their "on" time can impact receiver functionality far more than Eqn. 3 and 4 suggest.

In the remainder of this document, we develop new models for analyzing the impact of a gated, pulsed RFI source which take into account the time-varying nature of the overall pulsed waveform. In particular, we develop one model which allows us to characterize the average number of cycle slips per second as a function of the gated, pulsed RFI parameters, and another model which allows us to assess the probability of a bit error in data demodulation schemes. We compare the results of these models to the corresponding results obtained by using the DDCF degradation model of Eqn. 3 and 4, and we effectively show that the time-varying models often predict much worse performance than the DDCF counterparts. We present our results for a variety of gating duty

cycles, pulsed waveform duty cycles, and nominal C/N_0 values to illustrate the large range of differences between the two models.

2 Probabilistic Model for Cycle Slips

Cycle slips are an important measure of GPS receiver performance [5]. They occur when the phase estimate of the carrier waveform shifts by 360°. This offset is important as it degrades the accuracy of a PNT solution. Moreover, when the incoming signal is encoded with data, cycle slips (now of 180°) can cause *data bit inversions*, thus creating bit errors. Here we present a model for assessing the *average number of cycle slips per second* (ACS) as a means of quantifying cycle slip performance, which, as we shall see, is largely linked to C/N_0.

When C/N_0 is constant, the number of cycle slips k in a a period of time t is Poisson distributed [4, 5]. Specifically, if we denote by $Pr\{k(t)\}$ the probability of k cycle slips occurring in t seconds, we have

$$\Pr\{k(t)\} = \frac{\left(\frac{t}{\bar{T}_{CS}}\right)^k \exp\left(-\frac{t}{\bar{T}_{CS}}\right)}{k!} \tag{5}$$

$$\bar{T}_{CS} = \frac{\pi \tanh(\pi\theta_e\Psi)}{2B_L\theta_e}\left[I_0^2(\Psi) + 2\sum_{n=1}^{\infty}(-1)^n \frac{I_n^2(\Psi)}{1+\left(\frac{n}{\Psi\theta_e}\right)^2}\right]\Bigg|_{\Psi=\zeta\left(\frac{p}{2\pi\sigma_\phi}\right)^2} \tag{6}$$

where $\bar{T}_{CS}$ is called the *mean time to cycle slip*, and the parameters in Eqn. 6 are as listed in the table below:

- θ_e: steady-state jerk angle.
- B_L: one sided loop bandwidth.
- ζ: third order implementation loss.
- p: period of equivalent S-curve of tracking loop.
- σ_ϕ: RMS phase error of tracking loop.
- $I_n()$: $n-$th order modified Bessel function of the first kind.

For carrier tracking, the parameter σ_ϕ above is given by

$$\sigma_\phi = \sqrt{\sigma_t^2 + \sigma_R^2 + \sigma_T^2} \tag{7}$$

$$\sigma_t = \sqrt{\frac{B_L}{(C/N_0)}\left(1 + \frac{1}{2T_L(C/N_0)}\right)}. \tag{8}$$

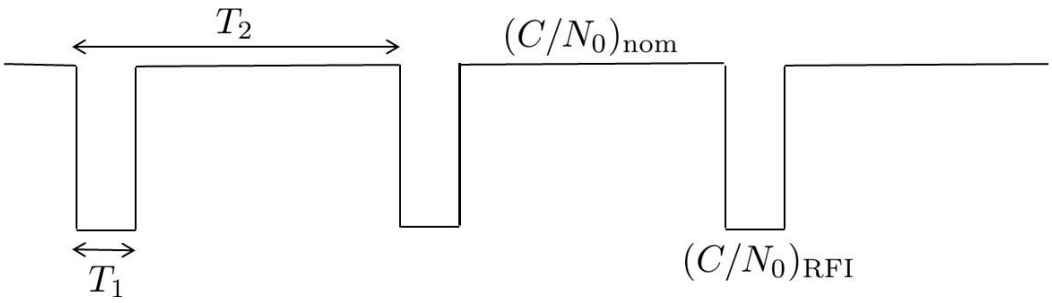

Figure 3: Graphical depiction of periodically varying C/N_0 for a low frequency gating waveform.

In Eqn. 7 and 8, T_L refers to the coherent integration time, and σ_R and σ_T refer to the receiver and satellite RMS noise levels, respectively. It is clear from Eqn. 8 that the RMS phase error is highly a function of C/N_0. In particular, as C/N_0 decreases, σ_ϕ increases, and $\bar{T}_{CS}$ decreases, meaning that cycle slips become more frequent.

By virtue of the Poisson distribution in Eqn. 5, the expected number of cycle slips in a given time $E\{k(t)\}$ is

$$E\{k(t)\} = \frac{t}{\bar{T}_{CS}} \tag{9}$$

Observe that the expected number of cycle slips grows linearly with time. We define ACS, the average number of cycle slips per second, as the long-term average of the expected number of cycle slips:

$$ACS \triangleq \lim_{t\to\infty} \frac{E\{k(t)\}}{t} = \frac{1}{\bar{T}_{CS}}. \tag{10}$$

When C/N_0 is constant, Eqn. 10 tell us that the ACS is simply the reciprocal of the mean-time-to-cycle slip, an intuitive result.

2.1 ACS for Periodically Varying C/N_0

We model the effect of gating on the high frequency pulsed waveform by considering C/N_0 that is periodically varying, as depicted in Fig. 3. When pulsed RFI is not present (corresponding to the case when the rotating antenna is not illuminating the GPS receiver), then the value of C/N_0 is some nominal value $(C/N_0)_{\text{nom}}$. When the pulsed RFI is present, the effective noise level increases, and C/N_0 is lowered for T_1 seconds to a value we denote as $(C/N_0)_{\text{RFI}}$. This process repeats periodically with period T_2. In terms of the NASA SMAP example discussed in the introduction, $T_1 = \tau_{obs}$ and $T_2 = T_{TC}$ (refer to Eqn. 4).

To derive an expression for the ACS in this new scenario, we first need to model the probability that k cycle slips occur in a given time t. Because C/N_0 now varies with time, the simple Poisson model of Eqn. 5 does not directly apply. To begin, let us first find the probability mass function for the number of cycle slips k that occur in one period of the C/N_0 waveform T_2. To aid us in our computation, it is helpful to partition the time length T_2 into two separate regions: a region of length T_1 where $C/N_0 = (C/N_0)_{\text{RFI}}$ and a region of length $T_2 - T_1$ where $C/N_0 = (C/N_0)_{\text{nom}}$.

Observe now that the following equality holds

$$\Pr\{k(T_2)\} = \sum_{m=0}^{k} \Pr\{m(T_1)\}\Pr\{(k-m)(T_2-T_1)\} \tag{11}$$

The above relationship says the following: suppose that a total of cycle slips that occurs in time T_2 is k, and that of these k cycle slips, m of them occur in the first T_1 seconds. It follows then that $k-m$ cycle slips occur in the remaining time $T_2 - T_1$. The probability that k cycle slips occurs in time T_2 is therefore the sum over all possible combinations of having m cycle slips occur in time T_1 and $k-m$ cycle slips occur in T_2. Observe that because C/N_0 is constant over each interval:

$$\Pr\{m(T_1)\} = \frac{\left(\frac{T_1}{\bar{T}_{CS_{\text{RFI}}}}\right)^m \exp\left(-\frac{T_1}{\bar{T}_{CS_{\text{RFI}}}}\right)}{m!} \tag{12}$$

$$\Pr\{(k-m)(T_2-T_1)\} = \frac{\left(\frac{T_2-T_1}{\bar{T}_{CS_{\text{nom}}}}\right)^{k-m} \exp\left(-\frac{T_2-T_1}{\bar{T}_{CS_{\text{nom}}}}\right)}{(k-m)!} \tag{13}$$

Substituting Eqn. 12 and 13 into Eqn. 11 and evaluating the sum yields

$$\Pr\{k(T_2)\} = \frac{\mu^k \exp(-\mu)}{k!} \tag{14}$$

$$\mu = \frac{T_1}{\bar{T}_{CS_{\text{RFI}}}} + \frac{T_2-T_1}{\bar{T}_{CS_{\text{nom}}}}. \tag{15}$$

The above result is likely familiar to those who know queuing theory, as it is simply a restatement that independent Poisson processes regenerate under addition. Those seeking a proof of this statement are referred the Appendix. While the probability mass function (PMF) for the number of cycle slips is not Poisson for an arbitrary time t, it *behaves* as a Poisson random variable when the time interval under consideration is the period length T_2. Moreover, it can be shown that for integer multiples n of the period length T_2 (see the Appendix for a proof):

$$\Pr\{k(nT_2)\} = \frac{\mu^k \exp(-\mu)}{k!} \tag{16}$$

$$\mu = \frac{nT_1}{\bar{T}_{CS_{\text{RFI}}}} + \frac{n(T_2-T_1)}{\bar{T}_{CS_{\text{nom}}}}. \tag{17}$$

A direct result of Eqn. 16 is that $E\{k(nT_2)\} = \mu$ of Eqn. 17. We can use this result to compute the ACS for the time-varying C/N_0 waveform. We are interested in computing

$$ACS = \lim_{t\to\infty} \frac{E\{k(t)\}}{t}. \tag{18}$$

To compute this limit, we first note that the $E\{k(t)\}$ is monotonically increasing with t. Indeed, because the arrival times of individual cycle slips are modeled as independent, then whenever $t_2 > t_1$,

$$E\{k(t_2)\} = E\{k(t_1)\} + E\{k(t_2-t_1)\} \geq E\{k(t_1)\}. \tag{19}$$

In particular, whenever $nT_2 \leq t \leq (n+1)T_2$, it follows that $E\{k(nT_2)\} \leq E\{k(t)\} \leq E\{k\left((n+1)T_2\right)\}$ and, moreover, that

$$\frac{E\{k(nT_2)\}}{(n+1)T_2} \leq \frac{E\{k(t)\}}{t} \leq \frac{E\{k\left((n+1)T_2\right)\}}{nT_2}. \tag{20}$$

By the squeeze theorem,

$$\lim_{n\to\infty} \frac{E\{k(nT_2)\}}{(n+1)T_2} \leq \lim_{t\to\infty} \frac{E\{k(t)\}}{t} \leq \lim_{n\to\infty} \frac{E\{k\left((n+1)T_2\right)\}}{nT_2}. \tag{21}$$

Utilizing Eqn. 17, we find that

$$\lim_{n\to\infty} \frac{E\{k(nT_2)\}}{(n+1)T_2} = \lim_{n\to\infty} \frac{E\{k\left((n+1)T_2\right)\}}{nT_2} = \frac{\frac{T_1}{T_2}}{\bar{T}_{CS_{\text{RFI}}}} + \frac{1-\frac{T_1}{T_2}}{\bar{T}_{CS_{\text{nom}}}} \tag{22}$$

which, by virtue of the inequality chain in Eqn. 21, leads to

$$ACS = \lim_{t\to\infty} \frac{E\{k(t)\}}{t} = \frac{\frac{T_1}{T_2}}{\bar{T}_{CS_{\text{RFI}}}} + \frac{1-\frac{T_1}{T_2}}{\bar{T}_{CS_{\text{nom}}}} \tag{23}$$

The result of Eqn. 23 has a somewhat intuitive appeal. If we define the variables

$$ACS_{\text{nom}} \triangleq \frac{1}{\bar{T}_{CS_{\text{nom}}}} \tag{24}$$

$$ACS_{\text{RFI}} \triangleq \frac{1}{\bar{T}_{CS_{\text{RFI}}}} \tag{25}$$

then Eqn. 23 is equivalent to

$$\boxed{ACS_{\text{eff}} = \frac{T_1}{T_2} ACS_{\text{RFI}} + \left(1-\frac{T_1}{T_2}\right) ACS_{\text{nom}}.} \tag{26}$$

where the "eff" subscript is used to denote the effective ACS of the time-varying model. Eqn. 26 states that the effective ACS when C/N_0 varies periodically is a weighted average of two *time-invariant* ACS's, one corresponding to the nominal C/N_0 and one corresponding to the C/N_0 during the pulsed interference.

2.2 Procedure for Comparing ACS: Time-varying Model vs. Average C/N_0 Model

We now describe the method for computing ACS_{eff} using our time-varying model and compare it to the ACS_{DDCF}, the ACS that is predicted by the DDCF model of Eqn. 3 and 4. After describing the general methods in both cases, we shall present results for a variety of case studies.

2.2.1 Computing ACS Using Time-varying Model (Eqn. 26)

As mentioned in the introduction, ITU-R Report M.2030 provides a model for computing the degradation in C/N_0 when non-gated, pulsed RFI is present (repeated here for convenience):

$$\Delta C/N_0 = 20\log(1 - PDC) \tag{27}$$

where PDC is the duty cycle of the high frequency, pulsed RFI signal. To compute ACS using the time-varying model of Eqn. 26, we use the following procedure:

- For a nominal value of $(C/N_0)_{\text{nom}}$ (when the pulsing is turned off by the gating waveform), compute $\bar{T}_{CS_{\text{nom}}}$ using Eqn. 6.
- Use the computed value of $\bar{T}_{CS_{\text{nom}}}$ to compute ACS_{nom} via Eqn. 10.
- For a given value of PDC, compute $(C/N_0)_{\text{RFI}} = (C/N_0)_{\text{nom}} + \Delta C/N_0$, where $\Delta C/N_0$ is computed via Eqn. 27.
- Use $(C/N_0)_{\text{RFI}}$ to compute $\bar{T}_{CS_{\text{RFI}}}$ via Eqn. 6 and then ACS_{RFI} via Eqn. 10.
- For given values of $T_1 = \tau_{obs}$ and $T_2 = T_{TC}$, compute ACS_{eff} via Eqn. 26.

2.2.2 Computing ACS Using the DDCF Model (Eqn. 3 and 4)

Also mentioned in the introduction, ITU-R Report M.2220 [2] and ITU-R Recommendation M.2030 [1] provide a model for computing degradation in C/N_0 when gated, pulsed RFI is present (repeated here for convenience):

$$\Delta C/N_0 = 20\log(1 - PDC_{LIM}) \tag{28}$$

$$PDC_{LIM} \triangleq PDC\frac{\tau_{obs}}{T_{TC}}. \tag{29}$$

where PDC is the duty cycle of the high frequency pulsed RFI waveform, T_{TC} is the period of the gating waveform, and τ_{obs} is the amount of time during one gating period for which the pulsed RFI is present. To compute ACS using the DDCF model (denoted ACS_{DDCF}), we use the following procedure:

- For given values of PDC, τ_{obs} and T_{TC}, compute $(C/N_0)_{\text{DDCF}} = (C/N_0)_{\text{nom}} - \Delta C/N_0$, where $\Delta C/N_0$ is computed via Eqn. 28 and 29.
- Using the calculated value of $(C/N_0)_{\text{DDCF}}$, compute $\bar{T}_{CS_{\text{DDCF}}}$ via Eqn. 6.
- Using the calculated value of $\bar{T}_{CS_{\text{DDCF}}}$, compute ACS_{DDCF} via Eqn. 10.

Parameter	Value
θ_e	0.7°
B_L	10Hz
ζ	−1.0dB
p	2π, Pilot Tone π, with Data
T_L	20msec
σ_R	2.9°
σ_T	2.2°

Table 1: Parameter values used in ACS calculations that were used to generate Fig. 4 through Fig. 7.

2.2.3 Results

Figures 4 through 7 show the results of computing the ACS via the two different models for a variety of scenarios. In each plot, the horizontal axis represents the duty cycle of the pulsed waveform from 1% to 50%, and the vertical axis shows the corresponding ACS (the gating duty cycle is held constant for each plot). The dashed red waveform indicates the ACS predicted via the DDCF model, ACS_{DDCF}, whereas the blue waveform represents the ACS predicted by the time-varying model, ACS_{eff}. The nominal value of C/N_0 is shown in the caption for each plot, and the values for the various parameters that are inputs to Eqn. 6 for computing $\bar{T}_{CS}$ are shown in Table 1.

Two different signal scenarios are depicted in the figures. Fig. 4 and Fig. 5 show ACS results for the case where the signal being received is a pilot tone (no data modulation). Such a scenario is characteristic of L2C receivers. In this case, a cycle slip occurs when a full 2π radians of phase error has accumulated, which accounts for the choice of $p = 2\pi$ in Table 1. By contrast, Fig. 6 and Fig. 7 depict ACS results when the received signal has modulated data. In this case, a cycle slip can occur only after π radians of phase error (due to ambiguity of the data bit multiplication of ± 1).

Some comments are in order. First, observe that whenever the gating duty cycle is 100%, the two models produce the exact same result. Such is to be expected since the original (non-gated) pulsed RFI waveform is obtained whenever gating is 100%. Also, observe that whenever PDC is small, the two models also effectively produce the same results (when PDC is zero, there is no pulsed RFI, and the two models should again produce identical results). As PDC increases from zero, the two models produce strikingly different results, with the time-varying model producing significantly higher estimates ACS_{eff} than that of ACS than the DDCF model ACS_{DDCF}. This effect is most notable for small gating duty cycles (e.g., 7%), but is also pronounced for moderate gating duty cycles (e.g., 25%) as well.

Overall, the depicted results indicate that the DDCF model may be overly optimistic in predicting ACS. While some simulated and/or measured data should be obtained to verify the time-varying model developed here, at the very least, the results suggest that one should use extreme caution in applying the DDCF model for PDC values that are more than a few percent.

Figure 4: ACS_{eff} vs. ACS_{DDCF} for a pilot tone, $(C/N_0)_{\text{nom}}$ = 30dB

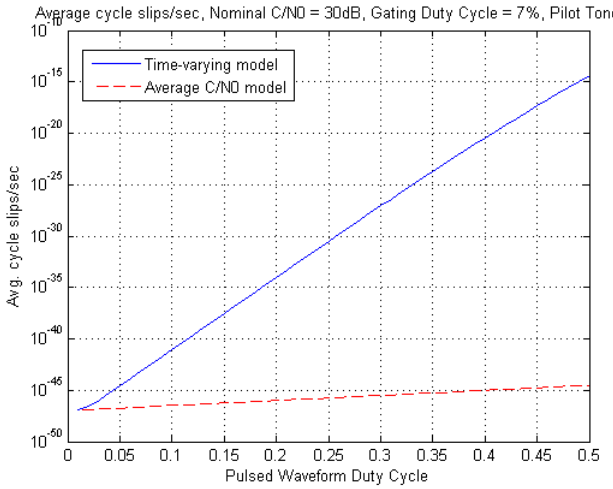

(a) Pilot Tone, Gating Duty Cycle = 7%

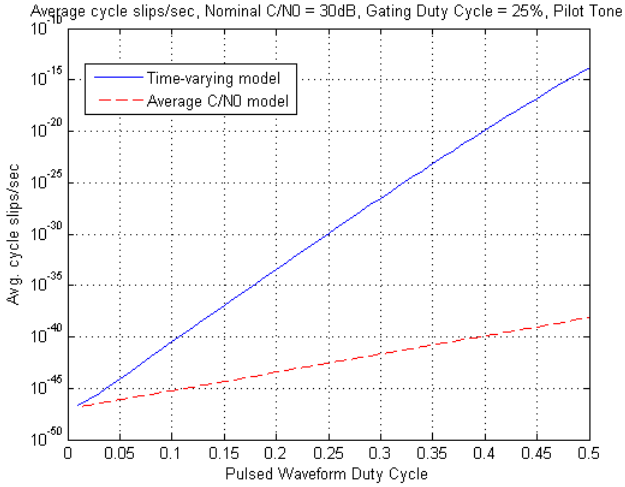

(b) Pilot Tone, Gating Duty Cycle = 25%

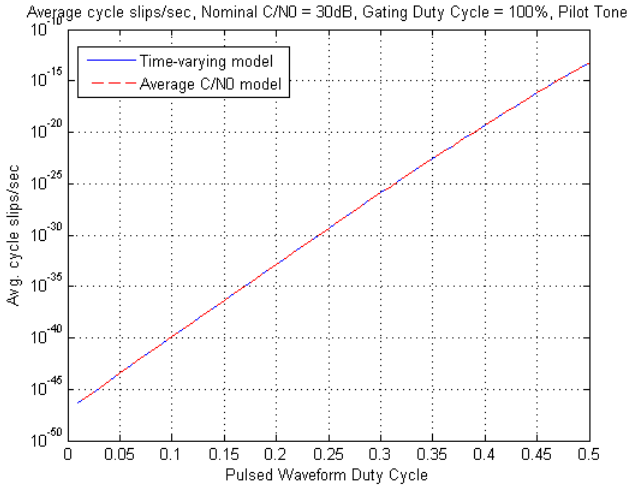

(c) Pilot Tone, Gating Duty Cycle = 100%

Figure 5: ACS_{eff} vs. ACS_{DDCF} for a pilot tone, $(C/N_0)_{\text{nom}}$ = 25dB

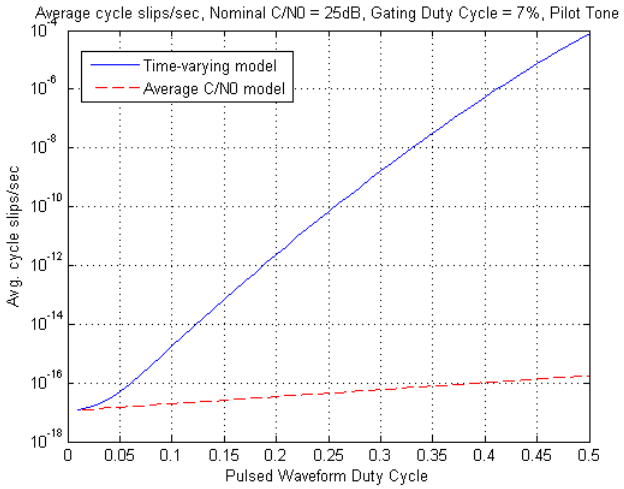

(a) Pilot Tone, Gating Duty Cycle = 7%

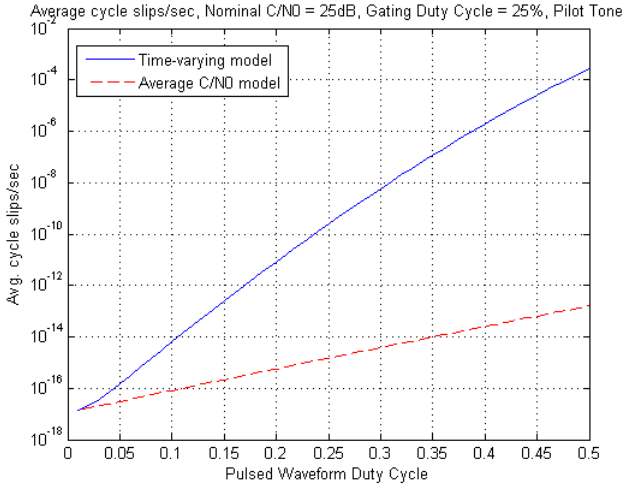

(b) Pilot Tone, Gating Duty Cycle = 25%

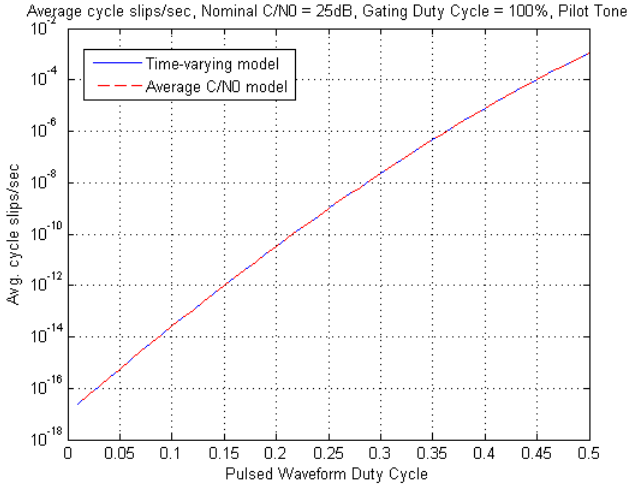

(c) Pilot Tone, Gating Duty Cycle = 100%

Figure 6: ACS_{eff} vs. ACS_{DDCF} for a data-modulated signal, $(C/N_0)_{\text{nom}}$ = 30dB

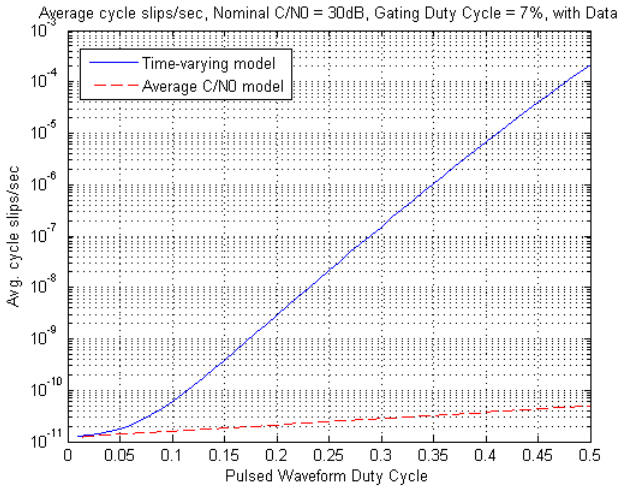

(a) Data-modulated, Gating Duty Cycle = 7%

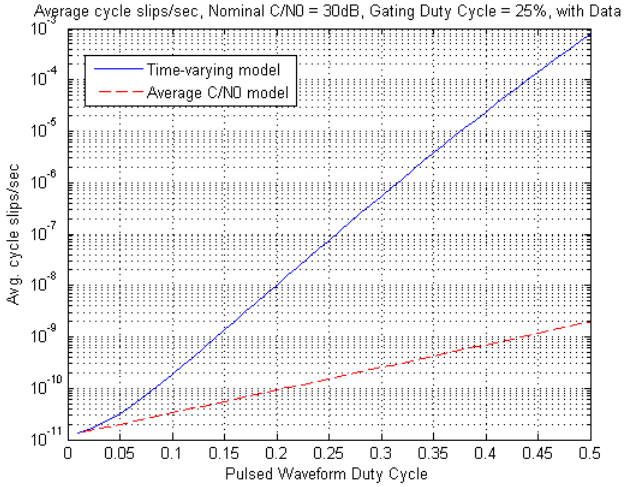

(b) Data-modulated, Gating Duty Cycle = 25%

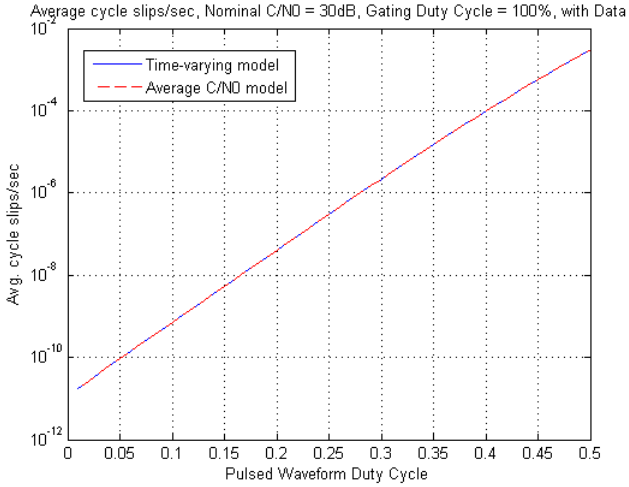

(c) Data-modulated, Gating Duty Cycle = 100%

Figure 7: ACS_{eff} vs. ACS_{DDCF} for a data-modulated signal, $(C/N_0)_{\text{nom}}$ = 25dB

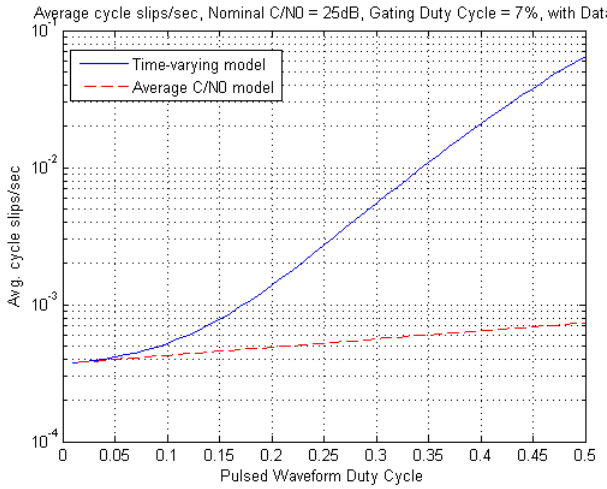

(a) Data-modulated, Gating Duty Cycle = 7%

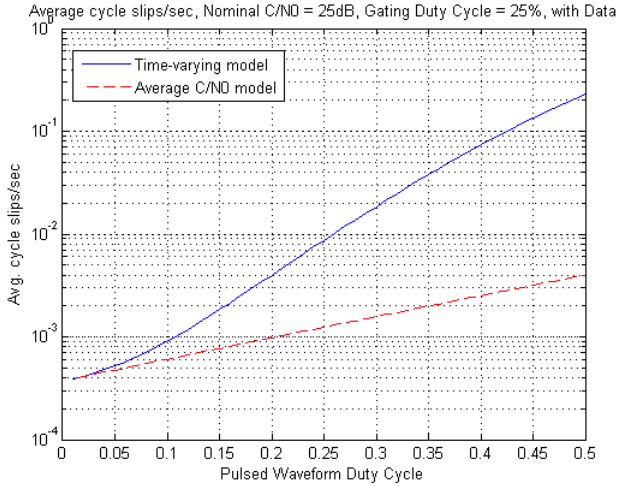

(b) Data-modulated, Gating Duty Cycle = 25%

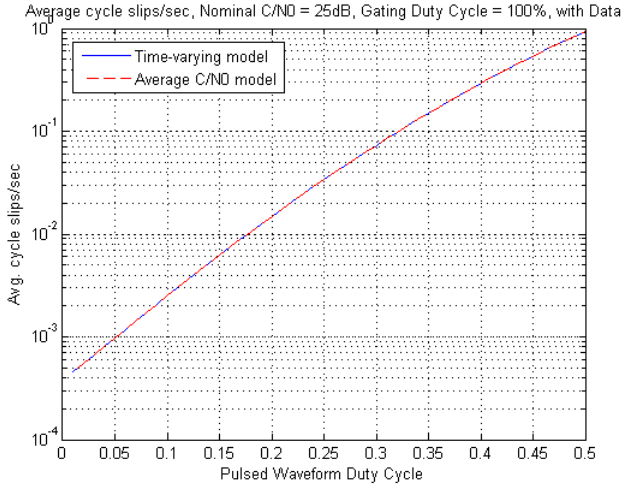

(c) Data-modulated, Gating Duty Cycle = 100%

3 Bit Error Probability for L1 C/A and P(Y) Codes

We now turn our attention to modeling the effect of gated, pulsed RFI on *data bit errors*. The cycle slip analysis of the previous section provides us some insight into how time-varying C/N_0 will affect the probability of bit errors (cycle slips will cause data bit inversions on data modulated channels). Here we perform a direct analysis of data bit error probability for a specific scenario, namely L1 C/A (or P(Y) code) which uses a (32,26) Hamming code to decode the data. In this particular case, for constant C/N_0, the probability of a bit error conditioned on knowledge of carrier phase error ϕ_e is given by [5]

$$P_{B|\phi_e} = \frac{1}{2}\text{erfc}\left(\frac{(C/N_0)\cos^2\phi_e}{R_B}\right) \tag{30}$$

where R_B is the bit transmission rate. The carrier phase error ϕ_e is itself a random variable with PDF [5].

$$p(\phi_e) = \frac{\exp\left(\frac{\cos(\phi_e-\theta_e)}{\sigma_\phi^2}\right)}{2\pi I_0\left(\frac{1}{\sigma_\phi^2}\right)}, \qquad |\phi_e| \le \pi. \tag{31}$$

where, again, σ_ϕ^2 is computed via Eqn. 7 and 8. The average probability of bit error is thus

$$P_B = \int_{-\pi}^{\pi} P_{B|\phi_e} p(\phi_e) d\phi_e. \tag{32}$$

When C/N_0 is piecewise constant, as in Fig. 3, we can compute the average probability of error using Bayes' Rule. Suppose we denote by P_B^{nom} the average probability of a bit error when $C/N_0 = (C/N_0)_{\text{nom}}$, and P_B^{RFI} as the average probability of a bit error when $C/N_0 = (C/N_0)_{\text{RFI}}$. Then the effective average probability of a bit error P_B^{eff} is given by

$$\begin{aligned} P_B^{\text{eff}} &= P_B^{\text{RFI}} P\{C/N_0 = (C/N_0)_{\text{RFI}}\} + P_B^{\text{nom}} P\{C/N_0 = (C/N_0)_{\text{nom}}\} \\ &= \boxed{P_B^{\text{RFI}} \frac{T_1}{T_2} + P_B^{\text{nom}}\left(1 - \frac{T_1}{T_2}\right).} \end{aligned} \tag{33}$$

3.1 Procedure for Comparing Average Bit Error Probability: Time-varying Model vs. Average C/N_0 model

The procedure we use to compare the average bit error probability obtained via the time-varying model to that obtained by the DDCF model is very similar to the procedure for comparing ACS for the two models. We describe the exact procedures here and then present results for a variety of case studies.

3.1.1 Computing Average Probability of Bit Error for Time-varying Model (Eqn. 34)

- For a nomminal value of $(C/N_0)_{\text{nom}}$ (when the pulsing is turned off by the gating waveform), compute σ_ϕ via Eqn. 7 and 8.

Parameter	Value
θ_e	0.35°
B_L	10Hz
T_L	10msec
σ_R	2.9°
σ_T	2.2°
R_B	50 bits/sec

Table 2: Parameter values used in P_B calculations that were used to generate Fig. 8 and Fig. 9.

- Substitute the computed value of σ_ϕ into Eqn. 30 and use this to compute P_B^{eff} via Eqn. 32.
- For a given value of PDC, compute $(C/N_0)_{\text{RFI}} = (C/N_0)_{\text{nom}} + \Delta C/N_0$, where $\Delta C/N_0$ is computed via Eqn. 27.
- Use $(C/N_0)_{\text{RFI}}$ to compute the corresponding value of σ_ϕ via Eqn. 7 and 8, and use this value to compute P_B^{RFI} via Eqn. 32.
- For given values of $T_1 = \tau_{obs}$ and $T_2 = T_{TC}$, compute P_B^{eff} via Eqn. 34.

3.1.2 Computing Average Bit Error Probability Using DDCF Model (Eqn. 3 and 4)

The procedure for computing average bit error probability using the DDCF model, denoted by P_B^{DDCF}), is again very similar to the procedure for computing ACS using the DDCF model:

- For given values of PDC, τ_{obs} and T_{TC}, compute $(C/N_0)_{\text{DDCF}} = (C/N_0)_{\text{nom}} + \Delta C/N_0$, where $\Delta C/N_0$ is computed via Eqn. 28 and 29.
- Using the calculated value of $(C/N_0)_{\text{DDCF}}$, compute the corresponding value of σ_ϕ via Eqn. 7 and 8.
- Substitute σ_ϕ into Eqn. 30, and use this expression to compute P_B^{DDCF} via Eqn. 34.

3.2 Results

Figures 8 and 9 depict the results of computing the average bit error probability for two different scenarios. As before, the horizontal axis in each plot represents the duty cycle of the pulsed waveform from 1% to 50%, and the vertical axis shows the corresponding average bit error probability. The dashed red waveform depicts P_B^{DDCF} while the blue waveform depicts P_B^{eff} for the time-varying model. The nominal values of C/N_0 are shown in the caption for each plot, and the values for various parameters that inputs to the relevant equations are shown in Table 2.

The plots in Fig. 8 and Fig. 9 depict the same qualitative behavior as their ACS counterparts Fig. 4 through Fig. 7; the two models coincide for gating duty cycles of 100% and for pulse duty

cycles of 0%. Furthermore, for low gating duty cycles, P_B^{eff} quickly grows to be much larger than P_B^{DDCF} as PDC increases. Therefore, the same general conclusions and warnings apply to the average probability of bit error as for ACS: the DDCF model exhibits overly optimistic behavior, so extreme caution should be used when applying it for situations where the PDC values are more than a few percent.

4 Summary

Our goal in this document has been to evaluate the validity of the DDCF model that is currently present in ITU-R Recommendation M.2030 [1]. Using the average number of cycle slips per second and the average probability of a bit error as high-level performance indicators, we developed models which explicitly take into account the time-varying nature of the C/N_0 profile and compared their performance to the approximate DDCF model. Our results indicate that in several realistic scenarios, the newly developed time-varying models predict much worse performance than the corresponding DDCF model and, therefore, the applicability of the DDCF model should be questioned. Further analysis, either via simulation or laboratory measurement, is warranted to assess the validity of the time-varying models presented herein.

Figure 8: P_B^{eff} vs. P_B^{DDCF}, $(C/N_0)_{\text{nom}}$ = 30dB

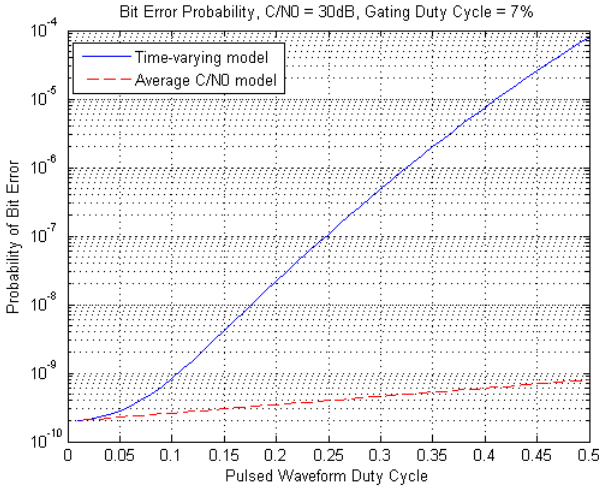

(a) Gating Duty Cycle = 7%

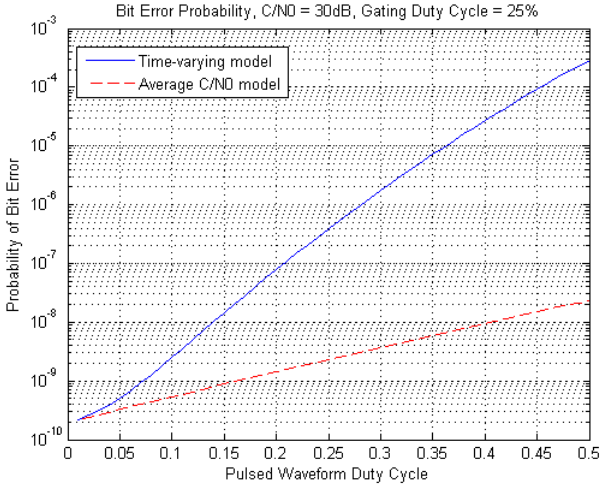

(b) Gating Duty Cycle = 25%

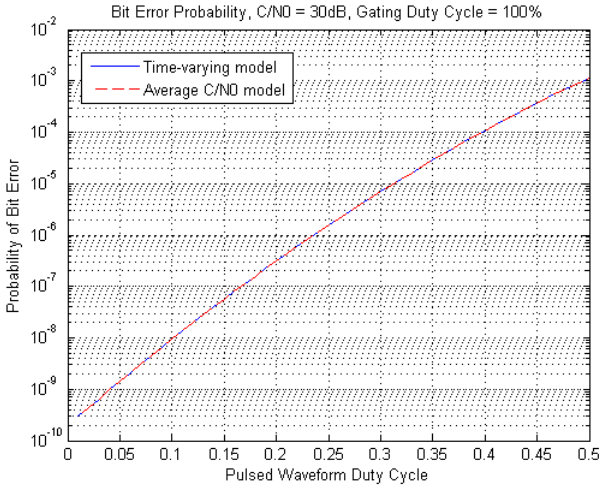

(c) Gating Duty Cycle = 100%

Figure 9: P_B^{eff} vs. P_B^{DDCF}, $(C/N_0)_{\text{nom}}$ = 25dB

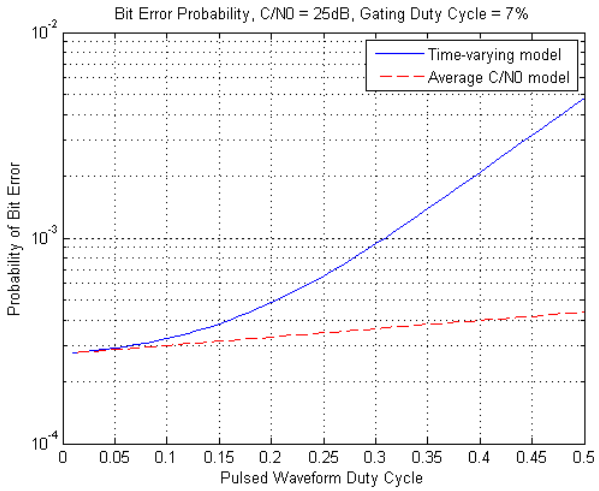

(a) Gating Duty Cycle = 7%

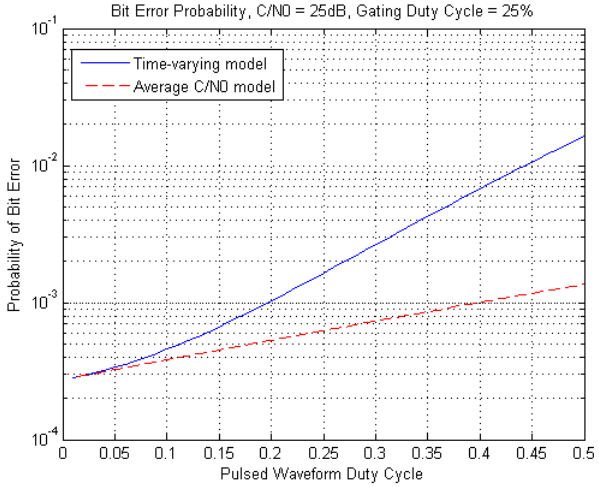

(b) Gating Duty Cycle = 25%

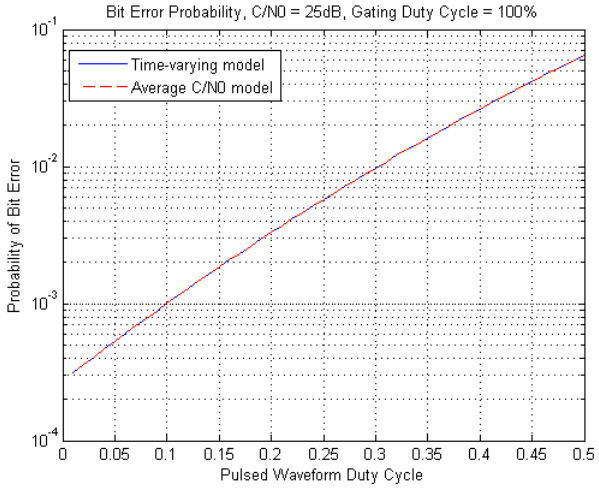

(c) Gating Duty Cycle = 100%

5 References

[1] Anon., "Evaluated method for pulsed interference from relevant radio sources other than in the radionavigation-satellite service to the radionavigation-satellite service systems and networks operating in the 1 164-1 215 MHz, 1 215- 1 300 MHz, and 1 559 - 1 610 MHz frequency bands," *Recommendation ITU-R M.2030*, ITU, Geneva, 2012.

[2] Anon., "Calculation method to determine aggregate interference parameters of pulsed RF systems operating in and near the bands 1 164-1 215 MHz and 1 215-1 300 MHz that may impact radionavigation-satellite service airborne and ground-based receivers oeprating in those frequency bands," *Report ITU-R M.2220*, ITU, Geneva, 2011.

[3] Anon., "Assessment of radio frequency interference relevant to the GNSS L5/E5A frequency band," *RTCA Report DO-292*, RTCA, Washington D.C., 2004.

[4] Anon., "Assessment of radio frequency interference relevant to the GNSS L1 frequency band," *RTCA Report DO-235B*, RTCA, Washington D.C., 2008.

[5] Anon., "Methodology and Criteria for Assessing GPS Radio Frequency Compatibility," Internal Technical Report, MITRE Corp., 2010.

[6] Anon., "Receiver Reference Assumption Document for Assessing GPS Radio Frequency Compatibility," Internal Technical Report, MITRE Corp., 2010.

[7] Grabowski J and Hegarty C, "Characterization of L5 Receiver Performance using Digital Pulse Blanking," *ION 15th International Technical Meeting of the Satellite Division Proceedings,* 1630-1635, Portland, 2002.

[8] Hegarty C, Van Dierendonck AJ, Bobyn D, Tran M, Kim T and Grabowski J, "Suppression of Pulsed Interference through Blanking," *Proceedings of the IAIN World Congress and 56th Meeting of ION*, 399-408, San Diego, 2000.

[9] Parl SA, and Shultz D, "Impact of Pulsed Interference on Spread Spectrum Receivers," Internal Technical Report, MITRE Corp., 2011.

[10] NASA SMAP website , `https://smap.jpl.nasa.gov`.

Appendix A

A.1 Proof of Eqn. 12 and 13

To simplify notation, we make the following definitions:

$$\alpha \triangleq \frac{T_1}{\bar{T}_{CS_{\text{RFI}}}} \tag{34}$$

$$\beta \triangleq \frac{T_2 - T_1}{\bar{T}_{CS_{\text{nom}}}}. \tag{35}$$

With the above substitutions, the sum of Eqn. 11 becomes

$$\sum_{m=0}^{k} \frac{\alpha^m e^{-\alpha}}{m!} \frac{\beta^{k-m} e^{-\beta}}{(k-m)!} = \beta^k e^{-(\alpha+\beta)} \sum_{m=0}^{k} \frac{\left(\frac{\alpha}{\beta}\right)^m}{m!(k-m)!} \tag{36}$$

$$= \frac{\beta^k e^{-(\alpha+\beta)}}{k!} \sum_{m=0}^{k} \frac{\left(\frac{\alpha}{\beta}\right)^m k!}{m!(k-m)!} \tag{37}$$

$$= \frac{\beta^k e^{-(\alpha+\beta)}}{k!} \sum_{m=0}^{k} \binom{k}{m} \left(\frac{\alpha}{\beta}\right)^m \tag{38}$$

$$= \frac{\beta^k e^{-(\alpha+\beta)}}{k!} \left(1 + \frac{\alpha}{\beta}\right)^k \tag{39}$$

$$= \frac{(\alpha+\beta)^k e^{-(\alpha+\beta)}}{k!} \tag{40}$$

Observe that the binomial theorem was applied in Eqn. 38 to obtain Eqn. 39. Noting that $\mu = \alpha + \beta$ completes the proof.

Implicit in the above derivation is the assumption that we consider a time interval of length T_2 which starts on the falling edge of the C/N_0 waveform of Fig. 3 and ends at the next falling edge. This assumption, however, is not critical and the result holds for an *arbitrary* interval of length T_2 as we now show. Suppose we consider an interval of length T_2 which starts t units of time before a falling edge of the C/N_0 waveform. Then the probability that k cycle slips occur in an interval that ends T_2 seconds after this starting time can be expressed as

$$\Pr\{k(T_2)\} = \sum_{m=0}^{k} \left(\sum_{n=0}^{m} \frac{\alpha^n e^{-\alpha}}{n!} \frac{\beta^{n-m} e^{-\beta}}{(n-m)!} \right) \frac{\gamma^{k-m} e^{-\gamma}}{(k-m)!} \tag{41}$$

$$\alpha \triangleq \frac{t}{\bar{T}_{CS_{\text{nom}}}} \tag{42}$$

$$\beta \triangleq \frac{T_1}{\bar{T}_{CS_{\text{RFI}}}} \tag{43}$$

$$\gamma \triangleq \frac{T_2 - T_1 - t}{\bar{T}_{CS_{\text{nom}}}}. \tag{44}$$

Observe now that

$$\Pr\{k(T_2)\} = \sum_{m=0}^{k}\left(\sum_{n=0}^{m}\frac{\alpha^n e^{-\alpha}}{n!}\frac{\beta^{n-m}e^{-\beta}}{(n-m)!}\right)\frac{\gamma^{k-m}e^{-\gamma}}{(k-m)!} \tag{45}$$

$$= \sum_{m=0}^{k}\frac{(\alpha+\beta)^m e^{-(\alpha+\beta)}}{m!}\frac{\gamma^{k-m}e^{-\gamma}}{(k-m)!} \tag{46}$$

$$= \frac{(\alpha+\beta+\gamma)^k e^{-(\alpha+\beta+\gamma)}}{k!}. \tag{47}$$

In the above, we have applied the first part of this proof twice in evaluating the sums. Noting that $\alpha+\beta+\gamma = \mu$, we see that Eqn. 47 is equivalent to Eqn. 14. A similar set of sums can be written for the situation that the initial starting point for the length T_2 interval lies between the falling edge of the C/N_0 waveform and the rising edge, and the result is exactly the same. Hence, Eqn. 14 and 15 represent the PMF for the number of cycle slips that occur in an arbitrary time interval of length T_2.

A.2 Proof of Eqn. 16 and 17

The proof of this statement is very similar to the last proof of Eqn. 14 and 15 and, hence, many of the details are omitted for brevity. Note that we have already proved the base case $n = 1$. Assuming the statement is true for some arbitrary value of n, then the probability that k cycle slips occur in time $(n+1)T_2$ can be expressed as

$$\Pr\{k\,((n+1)T_2)\} = \sum_{m=0}^{k}\Pr\{m\,(nT_2)\}\Pr\{(k-m)\,(T_2)\} \tag{48}$$

Stated in words, the probability that k cycle slips occur in time $(n+1)T_2$ is the probability that m cycle slips occur over the first nT_2 seconds followed by $k-m$ cycle slips occur in the following T_2 seconds, summed over all possible values of m. We have already established that the two quantities in the sum in Eqn. 48 are Poisson random variables. Hence, the same computation may be carried out as in the Proof of Eqn. 14 and 15 to show the general result.

Distribution List

Internal

J82C

Alessandro Cerruti

Michael Jeffris

Steen Parl

J82D

David Choi